applied sciences

MDPI

Article

Stability Analysis of the Vehicular Platoon with Sensing Delay and Communication Delay: CTCR Paradigm via Dixon Resultant

Xu Zhu [1,*], Yongming Shen [1], Zehua Zhang [2] and Maode Yan [1]

[1] School of Electronics and Control Engineering, Chang'an University, Xi'an 710064, China; ymshen@chd.edu.cn (Y.S.); mdyan@chd.edu.cn (M.Y.)
[2] School of Automation, Northwestern Polytechnical University, Xi'an 710129, China; m15594989537@163.com
* Correspondence: zx@chd.edu.cn

Abstract: For the vehicular platoon consisting of connected automotive vehicles, time delays degrade both the internal stability and string stability. In this study, the internal stability and string stability of the vehicular platoon suffering from sensing delay and communication delay are investigated. In the internal stability analysis, the necessary and sufficient internal stability condition is obtained and the exact time delay margins (ETDMs) are derived via the cluster treatment of characteristic root (CTCR) paradigm. A Dixon resultant matrix–based method is proposed to determine the kernel and offspring hypersurfaces of the CTCR paradigm, and then the computational burden of deriving the ETDMs is reduced significantly. In the string stability analysis, we first propose the string stability conditions for the situation no matter how large the frequency of the leader vehicle's maneuver is. Furthermore, the more practical string stability conditions are studied by considering only the region of low frequency, where most of the energy of the spacing errors exists. Then, a lower bound of the time headway is deduced to enhance road capacity, so the potential of the vehicular platoon is fully motivated. Numerical simulations are provided to illustrate the effectiveness of the theoretical claims.

Keywords: vehicular platoon; sensing delay; communication delay; internal stability; string stability; CTCR; time headway

check for updates

Citation: Zhu, X.; Shen, Y.; Zhang, Z.; Yan, M. Stability Analysis of the Vehicular Platoon with Sensing Delay and Communication Delay: CTCR Paradigm via Dixon Resultant. *Appl. Sci.* **2023**, *13*, 11807. https://doi.org/10.3390/app132111807

Academic Editors: Jianping Wu and Feng Zhu

Received: 4 September 2023
Revised: 26 October 2023
Accepted: 27 October 2023
Published: 28 October 2023

Copyright: © 2023 by the authors. Licensee MDPI, Basel, Switzerland. This article is an open access article distributed under the terms and conditions of the Creative Commons Attribution (CC BY) license (https://creativecommons.org/licenses/by/4.0/).

1. Introduction

Vehicular platoon technology is a promising approach to improving traffic capacity, enhancing highway safety, and reducing exhaust emissions and fuel consumption [1,2]. A vehicular platoon consists of a group of coordinated vehicles that are connected autonomously by using vehicle–to–vehicle (V2V) and vehicle–to–infrastructure (V2I) communication technologies [3]. To maintain a stable vehicular platoon, it is crucial to ensure both the internal stability and string stability [4]. The internal stability refers to the convergence of the trajectories of all the vehicles within the platoon [5]. On the other hand, the string stability implies that disturbances should not amplify when propagating along the vehicle string [6].

In the vehicular platoon, time delays are introduced due to the sensing time and limited communication bandwidth, which are unavoidable aspects of using the sensors and wireless communication [7,8]. These time delays are widely recognized as the primary factors that can significantly degrade the performance of the vehicular platoon and potentially lead to the internal instability or string instability [9]. Hence, it is essential to study the stability of the vehicular platoon with sensing delay and communication delay.

Numerous studies have been conducted on delay–dependent stability analysis of vehicular platoons. For investigating the internal stability of the system with multiple delays, both the exponential convergence rates of the system's states and delay margin are estimated by using the Lyapunov–Razumikhin theorem [10]. For the vehicular platoon with heterogeneous communication delays, the sufficient internal stability conditions are solved

by using the Lyapunov–Krasovskii method [11]. The Nyquist criterion has been utilized to investigate the internal stability affected by the communication delay and determine the maximum allowable time delay [12]. Most existing studies of analyzing the internal stability of the vehicular platoon with time delays rely on the Lyapunov–Razumikhin and Lyapunov–Krasovskii functions [13,14]. However, these studies can only obtain the sufficient stability conditions, rather than the necessary and sufficient conditions, resulting in relatively conservative results. Thus, the exact (non–conservative) time delay margins (ETDMs) could barely be solved using the above–mentioned methods. Additionally, since these studies involve solving the linear matrix inequalities, the computational burden exponentially increases with the dimension of the matrix.

For solving the ETDMs of the vehicular platoon, a crucial stability paradigm called cluster treatment of characteristic root (CTCR) is deployed in a different way [15]. The CTCR paradigm provides a comprehensive understanding of the loci of the purely imaginary characteristic roots of the closed–loop platoon dynamics and offers a systematic method of determining the exact and exhaustive stability for both the single–delay and multi–delay cases. These loci represent the potential delay margins in the delay space, and they are located on the kernel and offspring hypersurfaces within the CTCR paradigm. The CTCR paradigm enables a graphical representation of the delay margins and can be implemented numerically [16]. By combining the CTCR paradigm with the Rekasius transformation, a necessary and sufficient internal stability condition is derived for the vehicular platoon with time delays [17]. For the vehicular platoon under generic communication topologies with two time delays, a resultant matrix–based approach is proposed to determine the kernel and offspring hypersurfaces of the CTCR paradigm [18,19].

Though the CTCR paradigm can be used to derive the ETDMs of the vehicular platoon, it bears a heavy computational burden due to its numerical and time–consuming frequency sweeping process [20]. The frequency sweeping process involves high–dimensional matrix computation, and as the dimensions of the matrices in the CTCR paradigm increase, the computational burden grows exponentially. Specifically, the vehicular platoon with time delays is a third–order system (its states mainly include position, velocity, and acceleration) in essence. This naturally leads to high–dimensional matrix computation. Existing approaches of deriving the kernel and offspring hypersurfaces of the CTCR paradigm, such as the Sylvester resultant [21] and extended Kronecker summation [22], face this challenge. For example, the extended Kronecker summation method is preferable to be combined with the CTCR paradigm, but it needs to construct a high–order auxiliary characteristic equation (ACE). Thus, there is an urgent need for a more efficient and streamlined approach that can alleviate the computational burden while ensuring the accurate analysis of the ETDMs of the vehicular platoon.

In addition to the internal stability analysis, studying the string stability of the vehicular platoon with time delays is also an important research topic. The string stability conditions are obtained for a second–order vehicular platoon (its states mainly include position and velocity) with a single delay, and the thresholds of the controller parameters are further provided according to the delay margin [23]. For the vehicular platoon with communication delays, the string stability analysis is achieved by scaling the trigonometric functions with the delays [24]. The delay terms are approximated by using the second-order Taylor series expansion near zero to derive the necessary string stability conditions [25]. The Padé approximation, which offers better precision in approximating the delay terms compared to the Taylor series expansion, has been used to obtain the less conservative string stability conditions [26]. It is worth noting that the aforementioned string stability analysis methods primarily focus on the disturbances acting on the leader vehicle and often neglect any limitations on the frequencies of the spacing errors. However, in practical scenarios, the leader vehicle is typically constrained by the physical and mechanical factors, resulting in less frequent maneuvers. The low–frequency region contains a significant portion of the energy of the spacing errors, making it critical for the string stability analysis. Unfortunately, this aspect has been overlooked in the previous studies.

It is demonstrated that the traditional proportional controller, when applied to the predecessor–following (PF) topology with the constant distance (CD) policy, cannot guarantee the string stability of a vehicular platoon [23]. To address this issue, one possible solution is to adopt the constant time headway (CTH) policy, where the distance between the successive vehicles is adjusted based on the velocity of the following vehicles. The CTH policy has shown the improved string stability characteristics compared to the CD policy by increasing the time headway. However, increasing the time headway reduces road capacity and increases fuel consumption. Therefore, it is crucial to determine the minimum allowable time headway with a trade–off. For a second–order platoon with the CTH policy, a sliding-mode controller is designed to guarantee the string stability; meanwhile, the bound of the time headway is obtained by analyzing the sufficient string stability conditions [27]. In [28], the multiple–predecessor following (MPF) topology is used to represent the communication relationship between the followers, and it is proved that the bound of the time headway can be reduced by increasing the number of followers. Then, the communication delay is considered in the controller design of a third–order vehicular platoon, and a lower bound of the time headway, which can compensate for the effects of communications delays, is achieved by introducing the acceleration feedback [29].

The purpose of this paper is to analyze the internal stability and string stability of the vehicular platoon with sensing delay and communication delay under PF topology. For the internal stability analysis, a Dixon resultant matrix–based method instead of the well–known Sylvester resultant is proposed to determine the kernel and offspring hypersurfaces of the CTCR paradigm, and then the computational burden of deriving the ETDMs for the internal stability analysis is reduced elegantly. The above strength is also exhibited by comparative simulation. For the string stability analysis, we first consider the situation no matter how large the frequency of the leader vehicle's maneuver is. The sufficient string stability conditions are obtained, and the bound of the time headway is derived. Furthermore, different from [29], the more practical string stability conditions are studied by considering only the region of low frequency, where most of the energy of the spacing errors exists. Under the limitation of low frequency, a lower bound of the time headway is derived, which means that the road capacity can be further improved. The architecture of this paper is depicted in Figure 1.

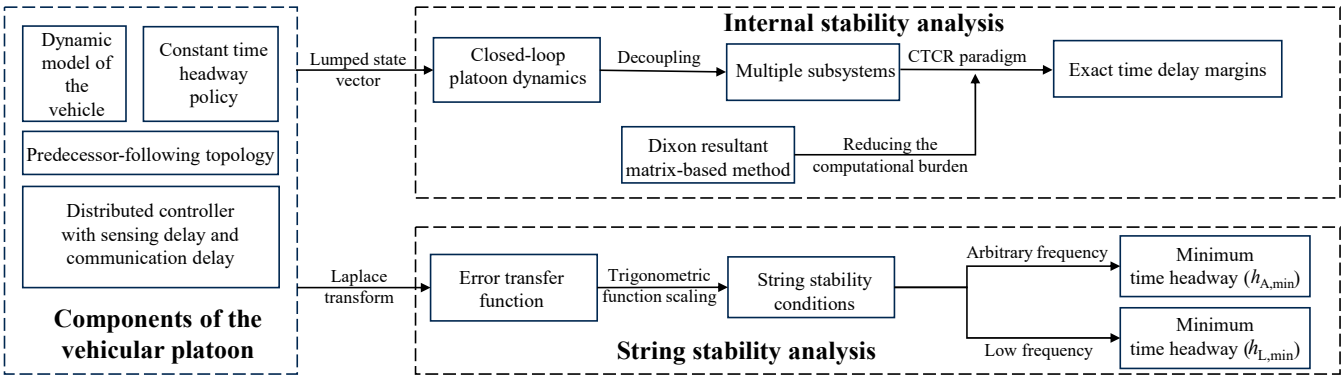


Figure 1. Architecture of the stability analysis of the vehicular platoon.

2. Problem Statement

2.1. Preliminaries

In this subsection, the model of the communication topology, definition of the Dixon resultant, and CTCR paradigm are demonstrated.

Firstly, the model of the communication topology is given. The platoon consists of one leader and N followers. In our work, the commonly used PF topology is chosen as the communication topology, as illustrated in Figure 2. The red arrows denote the transmission of information (i.e., position and velocity) through onboard sensors like radars, while the blue dashed arrows represent the transmission of information (i.e., acceleration) through

wireless communication networks. Furthermore, the integrated sensors are used to detect the position and velocity information of the preceding vehicle simultaneously, ensuring an identical sensing time for the above types of information [30].

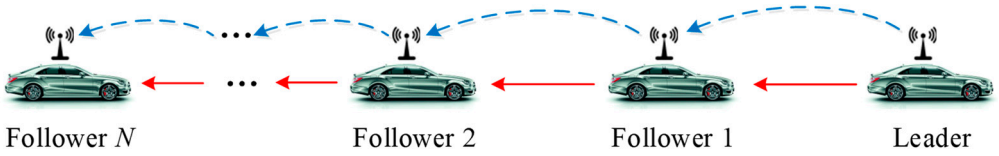


Figure 2. Predecessor–following topology.

The adjacent matrix of the PF topology is defined as

$$\mathcal{A} = [a_{ij}]_{N\times N} = \begin{bmatrix} 0 & 0 & & & \\ 1 & 0 & 0 & & \\ & \ddots & \ddots & \ddots & \\ & & 1 & 0 & 0 \\ & & & 1 & 0 \end{bmatrix}$$

where $a_{ij} = 1$ represents that the follower i can obtain information from the follower j; otherwise, $a_{ij} = 0$. $i = 1, 2, \cdots, N$, $j = 1, 2, \cdots, N$. The indegree matrix is characterized by $\mathcal{D} = \text{diag}\{\deg_1, \deg_2, \cdots, \deg_N\}$, $\deg_i = \sum_{j=1}^{N} a_{ij}$. According to the two above–mentioned matrices, the Laplacian matrix is modeled by $\mathcal{L} = \mathcal{D} - \mathcal{A}$. Then, the pinning matrix $\mathcal{P}$, which characterizes the information flow from the leader to the followers, is defined as

$$\mathcal{P} = [p_{ii}]_{N\times N} = \text{diag}\{1, 0, \cdots, 0\}$$

where $p_{ii} = 1$ represents that the follower i can receive the information from the leader; otherwise, $p_{ii} = 0$. We utilize the augmented Laplacian matrix $\widetilde{\mathcal{L}} = \mathcal{L} + \mathcal{P}$ to characterize the communication topology. For PF topology, every eigenvalue of $\widetilde{\mathcal{L}}$ is 1.

Secondly, the definition of the Dixon resultant is given. The Dixon resultant is a peer methodology to reveal the sufficient and necessary conditions of the nontrivial common solutions of the polynomial equations [31]. It outperforms the commonly used resultant formulation (i.e., Sylvester resultant) in computational efficiency [21]. The determinant of the Dixon resultant is equal to two polynomials, which can be used to implement the first step of the CTCR paradigm. The two polynomials are denoted as $\psi_1(x)$ and $\psi_2(x)$, where x is a variable. Then, the Dixon polynomial is given by

$$\mu(x, \alpha) = \frac{1}{(x-\alpha)} \begin{vmatrix} \psi_1(x) & \psi_2(x) \\ \psi_1(\alpha) & \psi_2(\alpha) \end{vmatrix} \tag{1}$$

where $\psi_1(\alpha)$ and $\psi_2(\alpha)$ stand for replacing x by a dummy variable α. $\mu(x, \alpha)$ is the degree of $d_{\max}$ in α, where $d_{\max} = \max[\deg(\psi_1(x))\deg(\psi_2(x))]$, and the notations $\deg(\psi_1(x))$ and $\deg(\psi_2(x))$ represent the degrees of $\psi_1(x)$ and $\psi_2(x)$ in x, respectively. As each common zero of $\psi_1(x)$ and $\psi_2(x)$ is also a zero of $\mu(x, \alpha)$ regardless of α values, the coefficient of each power product of α in $\mu(x, \alpha)$ should be zero at the common zero of $\psi_1(x)$ and $\psi_2(x)$. In view of this, $d_{\max}$ equations containing these coefficients are obtained as the polynomials in x. The coefficient matrix is called the Dixon matrix $D(\psi_1(x), \psi_2(x))$. Then, the $d_{\max}$ equations are written in the following form:

$$D(\psi_1(x), \psi_2(x)) \begin{pmatrix} 1 \\ x \\ \vdots \\ x^{d_{\max}-1} \end{pmatrix} = \begin{pmatrix} 0 \\ 0 \\ \vdots \\ 0 \end{pmatrix} \tag{2}$$

If there exists a nontrivial solution for $\psi_1(x)$ and $\psi_2(x)$, $D(\psi_1(x), \psi_2(x))$ must be singular [31].

$$\det[D(\psi_1(x), \psi_2(x))] = 0 \tag{3}$$

The determinant in (3) is called the Dixon resultant.

At last, some definitions of the CTCR paradigm are provided. The CTCR paradigm describes the knowledge of the complete loci of the purely imaginary characteristic roots in the delay space [15,32]. These loci are called "stability switching" hypersurfaces [33], which are the only possible stability switching locations. Therefore, the CTCR paradigm can be used to compute the purely imaginary characteristic roots and ETDMs by drawing the hypersurfaces. For more details about the CTCR paradigm refer to [15,32,33].

Definition 1. *Kernel hypersurfaces: The hypersurfaces contain all the delay points* (τ_1, τ_2)*, where an imaginary root* $(s = \iota \cdot \omega,\ \iota^2 = -1)$ *is created and the constraint* $0 < \tau_k \omega < 2\pi,\ k = 1, 2$ *is satisfied. The points on the kernel hypersurfaces contain the smallest delay compositions, which correspond to all possible imaginary roots.*

Definition 2. *Offspring hypersurfaces: The hypersurfaces are obtained from the kernel hypersurfaces by using the periodicity of the imaginary roots with respect to the delays. The points on the offspring hypersurfaces are easily derived from those on the kernel hypersurfaces by using the transformation*

$$\left\langle \left\{ \tau_1 + \frac{2\pi}{\omega} q_1, \tau_2 + \frac{2\pi}{\omega} q_2 \right\}, \omega \right\rangle \tag{4}$$

Definition 3. *Root tendency: For the imaginary roots* $\iota \cdot \omega,\ \iota^2 = -1$ *on the kernel hypersurfaces and offspring hypersurfaces, the root tendency of the delay* $\tau_k, k = 1, 2$ *is defined as*

$$\mathrm{RT}|_{s=\iota\cdot\omega}^{\tau_k} = \mathrm{sgn}\left[\mathrm{Re}\left(\frac{\partial s}{\partial \tau_k}\bigg|_{s=\iota\cdot\omega} \right) \right] \tag{5}$$

The root tendency RT depicts the direction of the root crossing across the kernel and offspring hypersurfaces as one of the delays increases infinitesimally. RT is -1 for stabilizing root crossing and $+1$ for destabilizing root crossing [34]. Then, by counting the number of the unstable characteristic roots of each region in the CTCR paradigm, the stable and unstable regions can be distinguished and the ETDMs are obtained.

2.2. Vehicle Dynamics and Platoon Control Objective

Within our framework, the longitudinal dynamics of the vehicles are denoted as

$$\begin{cases} \dot{r}_i(t) = v_i(t) \\ \dot{v}_i(t) = a_i(t) \\ \dot{a}_i(t) = -\frac{1}{T} a_i(t) + \frac{1}{T} u_i(t) \end{cases} \tag{6}$$

where $r_i(t)$, $v_i(t)$, $a_i(t)$ are the position, velocity, and acceleration of the i-th vehicle, respectively. $T > 0$ is the time constant of the drivetrain. The propelling force u_i represents the control input.

The longitudinal dynamics of the i-th vehicle can also be written in the state-space expression:

$$\dot{x}_i(t) = A x_i(t) + B u_i(t) \tag{7}$$

where $x_i(t) = [r_i(t),\ v_i(t),\ a_i(t)]^{\mathrm{T}}$ and

$$A = \begin{bmatrix} 0 & 1 & 0 \\ 0 & 0 & 1 \\ 0 & 0 & -\frac{1}{T} \end{bmatrix},\ B = \begin{bmatrix} 0 \\ 0 \\ \frac{1}{T} \end{bmatrix}$$

It is assumed that both the sensing delay and communication delay exist in the vehicular platoon. The objective of the platoon control under PF topology can be described as:

$$\begin{cases} r_i(t-\tau_1) \to r_{i-1}(t-\tau_1) - d - hv_i(t-\tau_1) \\ v_i(t-\tau_1) \to v_{i-1}(t-\tau_1) \\ a_i(t-\tau_2) \to a_{i-1}(t-\tau_2) \end{cases} \tag{8}$$

where τ_1, τ_2 are the sensing delay and communication delay, respectively. Our proposed delay structure is based on a realistic scenario in which the position and velocity can be sensed by the neighboring vehicles, while the acceleration is communicated through V2V communication. Then, these two different ways of acquiring information introduce two different delays [30]. To focus on deriving the ETDMs, we assume that τ_1, τ_2 are both constant. In reality, one may use a buffer memory to ensure that the sensing delay τ_1 and communication delay τ_2 are further delayed intentionally (if required) to be constant. Therein, we choose the CTH policy as the inter–vehicle spacing policy. d and h are the desired standstill spacing and time headway between two successive vehicles, respectively.

2.3. Closed–Loop Dynamics of the Vehicular Platoon with Sensing Delay and Communication Delay

According to the control objective (8), the spacing error of the i-th vehicle is represented as

$$e_i(t) = r_{i-1}(t) - r_i(t) - d - hv_i(t) \tag{9}$$

With respect to the sensing delay τ_1 and communication delay τ_2, the distributed controller is given by

$$\begin{aligned} u_i(t) = k_r[r_{i-1}(t-\tau_1) - r_i(t-\tau_1) - d - hv_i(t-\tau_1)] \\ +k_v[v_{i-1}(t-\tau_1) - v_i(t-\tau_1)] \\ +k_a[a_{i-1}(t-\tau_2) - a_i(t-\tau_2)] \end{aligned} \tag{10}$$

where $k_r > 0$, $k_v > 0$, $k_a > 0$ are the controller gains for position, velocity, and acceleration, respectively.

By applying the distributed controller (10) for the longitudinal vehicle dynamics (7), the governing equation with respect to the spacing error of the i-th follower is obtained as

$$\begin{aligned} &T\dddot{e}_i(t) + \ddot{e}_i(t) + k_a\ddot{e}_i(t-\tau_2) + (hk_r + k_v)\dot{e}_i(t-\tau_1) + k_re_i(t-\tau_1) \\ &= k_a\ddot{e}_{i-1}(t-\tau_2) + k_v\dot{e}_{i-1}(t-\tau_1) + k_re_i(t-\tau_1) \end{aligned} \tag{11}$$

The lumped error vector is defined as $e = [e_1, \cdots, e_N, \dot{e}_1, \cdots, \dot{e}_N, \ddot{e}_1, \cdots, \ddot{e}_N]^{\mathrm{T}}$. Thus, the closed–loop dynamics of the vehicular platoon can be written as

$$\dot{e}(t) = (A \otimes I_N)e(t) - [(BK_1) \otimes \widetilde{\mathcal{L}} + (hBK_2) \otimes I_N]e(t-\tau_1) - [(BK_3) \otimes \widetilde{\mathcal{L}}]e(t-\tau_2) \tag{12}$$

where I_N denotes the N-dimensional identity matrix, and $\otimes$ is the Kronecker product operation. $K_1 = [k_r, k_v, 0]$, $K_2 = [0, k_r, 0]$, $K_3 = [0, 0, k_a]$.

The characteristic polynomial of (12) is calculated as

$$
\begin{aligned}
f(s) &= \det\Big\{sI_{3N} - (A \otimes I_N) + [(BK_1) \otimes \widetilde{\mathcal{L}} + (hBK_2) \otimes I_N]\mathrm{e}^{-\tau_1 s} + [(BK_3) \otimes \widetilde{\mathcal{L}}]\mathrm{e}^{-\tau_2 s}\Big\} \\
&= \begin{vmatrix} sI_N & -I_N & 0_N \\ 0_N & sI_N & -I_N \\ \frac{k_r \mathrm{e}^{-\tau_1 s}}{T}\widetilde{\mathcal{L}} & \frac{k_v \mathrm{e}^{-\tau_1 s}}{T}\widetilde{\mathcal{L}} + \frac{hk_r \mathrm{e}^{-\tau_1 s}}{T} I_N & sI_N + \frac{1}{T} I_N + \frac{k_a \mathrm{e}^{-\tau_2 s}}{T}\widetilde{\mathcal{L}} \end{vmatrix} \\
&= \det(sI_N)\det\left(\begin{bmatrix} sI_N & -I_N \\ \frac{k_v \mathrm{e}^{-\tau_1 s}}{T}\widetilde{\mathcal{L}} + \frac{hk_r \mathrm{e}^{-\tau_1 s}}{T} I_N & sI_N + \frac{1}{T} I_N + \frac{k_a \mathrm{e}^{-\tau_2 s}}{T}\widetilde{\mathcal{L}} \end{bmatrix} - \begin{bmatrix} 0_N \\ \frac{k_r \mathrm{e}^{-\tau_1 s}}{T}\widetilde{\mathcal{L}} \end{bmatrix} (sI_N)^{-1} \begin{bmatrix} -I_N & 0_N \end{bmatrix}\right) \\
&= \det(sI_N)\det(sI_N)\det\Big[sI_N + \tfrac{1}{T} I_N + \tfrac{k_a \mathrm{e}^{-\tau_2 s}}{T}\widetilde{\mathcal{L}} - (\tfrac{k_v}{T}\widetilde{\mathcal{L}} + \tfrac{hk_r}{T} I_N + \tfrac{k_r}{sT}\widetilde{\mathcal{L}})\mathrm{e}^{-\tau_1 s}(sI_N)^{-1}(-I_N)\Big] \\
&= \prod_{i=1}^{N} [s^3 + \tfrac{1+k_a \mathrm{e}^{-\tau_2 s}}{T} s^2 + \tfrac{(k_v + hk_r)\mathrm{e}^{-\tau_1 s}}{T} s + \tfrac{k_r \mathrm{e}^{-\tau_1 s}}{T}]
\end{aligned} \tag{13}
$$

where s is the Laplace variable, and $\widetilde{\mathcal{L}}$ is a lower triangular matrix with all the elements of its diagonal being 1.

According to (13), the closed–loop platoon dynamics (12) can be decomposed into N subsystems. The characteristic equation of each subsystem is given by

$$
f_i(s) = s^3 + \frac{1 + k_a \mathrm{e}^{-\tau_2 s}}{T} s^2 + \frac{(k_v + hk_r)\mathrm{e}^{-\tau_1 s}}{T} s + \frac{k_r \mathrm{e}^{-\tau_1 s}}{T} \tag{14}
$$

3. Internal Stability Analysis

To reduce the computational burden of calculating the ETDMs of the vehicular platoon, we propose a Dixon resultant matrix-based method to determine the kernel and offspring hypersurfaces of the CTCR paradigm. In this section, it is shown that the dimension of our designed Dixon matrix is only half of that of the well–known Sylvester matrix.

The closed–loop platoon dynamics described by (12) should be primarily stable for the delay–free case [29]. Therefore, before analyzing the internal stability for the delay case, we first analyze the internal stability for the delay–free case, and a prerequisite is given.

For the delay-free case with $\tau_1 = \tau_2 = 0$, (14) becomes

$$
f_i(s) = s^3 + \frac{1 + k_a}{T} s^2 + \frac{k_v + hk_r}{T} s + \frac{k_r}{T} \tag{15}
$$

For a stable platoon, every $f_i(s) = 0$ in (15) should be Hurwitz stable. A lemma for the delay–free case is given as follows.

Lemma 1. *The closed-loop platoon dynamics (12) are internally stable for the delay–free case if the following inequality holds:*

$$
(1 + k_a)(k_v + hk_r) - Tk_r > 0 \tag{16}
$$

Proof. The stability of $f_i(s) = 0$ in (15) is easy to examine based on the Routh–Hurwitz stability criterion, shown in

$$
\begin{array}{lll}
s^3 & 1 & \frac{k_v + hk_r}{T} \\
s^2 & \frac{1+k_a}{T} & \frac{k_r}{T} \\
s^1 & \frac{(1+k_a)(k_v+hk_r) - Tk_r}{T(1+k_a)} & \\
s^0 & \frac{k_r}{T} &
\end{array} \tag{17}
$$

By considering the definition that $k_r > 0$, $k_v > 0$, $k_a > 0$ in (10), the inequality in (16) is derived. □

Remark 1. *Lemma 1 provides a necessary and sufficient internal stability condition of the closed–loop platoon dynamics described by (12) for the delay–free case, but it is just a necessary condition for the delay case. For* $\tau_1 > 0$ *and* $\tau_2 > 0$ *, the internal stability of the closed–loop platoon dynamics described by (12) not only relies on the control gains, but also depends on the sensing delay* τ_1 *and communication delay* τ_2 *.*

As the stability analysis procedure is identical for each subsystem, the subscript i is omitted afterward for clarity.

To establish the CTCR paradigm, we first replace the exponential terms in (14) by

$$\mathrm{e}^{-\iota\cdot\tau_k\omega} = \cos(\tau_k\omega) - \iota\cdot\sin(\tau_k\omega),\ k = 1, 2 \tag{18}$$

The cosine and sine functions are replaced by the half–angle tangent functions:

$$\cos(\tau_k\omega) = \frac{1 - z_k^2}{1 + z_k^2},\ \sin(\tau_k\omega) = \frac{2z_k}{1 + z_k^2},\ z_k = \tan\Big(\frac{\tau_k\omega}{2}\Big) \tag{19}$$

where z_k are the auxiliary variables.

Then, the infinite dimension polynomial (14) is transformed into a finite dimension polynomial in ω:

$$f(\omega, z_1, z_2) = \sum_{m=0}^{3} b_m(z_1, z_2)\omega^m + \iota\cdot\sum_{m=0}^{3} c_m(z_1, z_2)\omega^m \tag{20}$$

where $b_m(z_1, z_2)$ and $c_m(z_1, z_2)$ are the corresponding coefficients of ω.

If there exists an imaginary solution for (14) at $s = \iota\cdot\omega$, both the real and imaginary parts of (20) should be zero simultaneously:

$$\psi_1(\omega) = \mathrm{Re}(f(\omega, z_1, z_2)) = \sum_{m=0}^{3} b_m(z_1, z_2)\omega^m = 0 \tag{21a}$$

$$\psi_2(\omega) = \mathrm{Im}(f(\omega, z_1, z_2)) = \sum_{m=0}^{3} c_m(z_1, z_2)\omega^m = 0 \tag{21b}$$

To reduce the computational complexity, we choose the Dixon resultant instead of the popular Sylvester resultant to solve z_1, and z_2. The necessary condition for (21a) and (21b) to have a common imaginary root, i.e., $\iota\cdot\omega$, is described by the Dixon matrix $D(\psi_1(\omega), \psi_2(\omega))$ in (2). By scanning the parameters $\tau_1\omega$, $\tau_2\omega$ in $[0,\ 2\pi]$, the graphical description of $\tau_1\omega$, $\tau_2\omega$ is derived for the case that (3) holds. Then, the values of z_1, z_2 are obtained according to (19). The imaginary root $\iota\cdot\omega$ can be solved by substituting the values of z_1, z_2 into (21a) or (21b).

The Dixon resultant $D(\psi_1(\omega), \psi_2(\omega))$ constitutes a closed–form description of the kernel and offspring hypersurfaces of the CTCR paradigm. Next, by utilizing the remaining procedure of the CTCR paradigm, the ETDMs $< \overline{\tau}_1,\ \overline{\tau}_2 >$ are obtained. The remaining procedure of the CTCR paradigm is omitted here, and more details are presented in the literature [15,32,33].

Remark 2. *The Dixon resultant is computationally more efficient than the well–known Sylvester resultant and other popular methods (e.g., ACE combined with Kronecker summation* [22]*). Especially, for the third–order vehicular platoon with sensing delay and communication delay, the size of the Dixon matrix is just* 3×3*, but the sizes of the Sylvester matrix and ACE matrix are* 6×6 *and* 9×9*, respectively. Therefore, the Dixon resultant consumes less computational burden and is preferable to compute the ETDMs of the vehicular platoon.*

4. String Stability Analysis

By taking the Laplace transform of the governing Equation (11), the spacing error transfer function of the i-th vehicle is obtained as

$$G_i(s) = \frac{E_i(s)}{E_{i-1}(s)} = \frac{k_a s^2 \mathrm{e}^{-\tau_2 s} + k_v s \mathrm{e}^{-\tau_1 s} + k_r \mathrm{e}^{-\tau_1 s}}{Ts^3 + s^2 + k_a s^2 \mathrm{e}^{-\tau_2 s} + (hk_r + k_v) s \mathrm{e}^{-\tau_1 s} + k_r \mathrm{e}^{-\tau_1 s}} \tag{22}$$

where $E_i(s)$ is Laplace transform of the spacing error $e_i(t)$. $G_i(s)$ describes how the spacing error propagates upstream in the vehicular platoon. For a string–stable platoon, when the leader vehicle performs a sinusoidal acceleration maneuver at the frequency ω, there must exist [23]

$$|G_i(\iota \cdot \omega)| \leq 1 \tag{23}$$

Theorem 1. *For any scalar $\omega > 0$, the closed–loop platoon dynamics described by (12) are string–stable if one of the following conditions is satisfied.*

$$\Delta < 0 \ \wedge \beta_6 > 0 \ \wedge \beta_2 > 0 \tag{24a}$$

$$\Delta \geq 0 \ \wedge \beta_6 > 0 \ \wedge \beta_4 > 0 \ \wedge \beta_2 > 0 \tag{24b}$$

where

$$\begin{cases} \Delta = \beta_4^2 - 4Tk_r\beta_6\beta_2, \\ \beta_6 = T - 2k_a\tau_2, \\ \beta_4 = 1 - 2Thk_r - 2Tk_v - 2k_a - 2(Tk_r + hk_r + k_v)\tau_1 \\ \qquad -2hk_rk_a|\tau_2 - \tau_1|, \\ \beta_2 = h^2k_r + 2hk_v - 2. \end{cases}$$

With respect to the string stability conditions (24), the bound of the time headway is deduced by

$$h > h_{\mathrm{A,min}} = \frac{2(T + \tau_1)}{1 - 2k_a - 2Tk_r\tau_1} \tag{25}$$

Proof. We define $G_i(\iota \cdot \omega) = \frac{N}{N+M}$, where

$$\begin{cases} N = [-k_a\omega^2 \cos(\tau_2\omega) + k_v\omega \sin(\tau_1\omega) + k_r \cos(\tau_1\omega)] \\ \quad +\iota \cdot [k_a\omega^2 \sin(\tau_2\omega) + k_v\omega \cos(\tau_1\omega) - k_r \sin(\tau_1\omega)] \\ M = [-\omega^2 + hk_r\omega \sin(\tau_1\omega)] + \iota \cdot [-T\omega^3 + hk_r\omega \cos(\tau_1\omega)] \end{cases}$$

When the vehicular platoon is string stable as (23), there exists

$$\begin{aligned} |M+N|^2 - |N|^2 = {} & T^2\omega^6 - 2Tk_a\omega^5 \sin(\tau_2\omega) + \omega^4 - 2T(hk_r + k_v)\omega^4 \cos(\tau_1\omega) \\ & +2k_a\omega^4 \cos(\tau_2\omega) + 2(Tk_r - hk_r - k_v)\omega^3 \sin(\tau_1\omega) \\ & +2hk_rk_a\omega^3 \sin(\tau_2 - \tau_1)\omega + (h^2k_r^2 + 2hk_rk_v)\omega^2 \\ & -2k_r\omega^2 \cos(\tau_1\omega) \geq 0 \end{aligned} \tag{26}$$

According to the facts that $\pm \sin(\tau_k\omega) \geq -\tau_k\omega$ and $\pm \cos(\tau_k\omega) \geq -1$, $k = 1, 2$, it is obtained that

$$|M+N|^2 - |N|^2 \geq T\beta_6\omega^6 + \beta_4\omega^4 + k_r\beta_2\omega^2 \geq 0 \tag{27}$$

If one of the conditions (24) is satisfied, the inequality in (27) is fulfilled for $\omega > 0$.

Then, the bound of the time headway is deduced by (24b). When (24b) is satisfied, $\beta_2 > 0$ and $\beta_4 > 0$ can be rewritten as

$$k_v > \frac{1}{h} - \frac{hk_r}{2} \tag{28a}$$

$$k_v < \frac{1 - 2k_a - 2Tk_r\tau_1 - 2hk_r(T + \tau_1 + k_a|\tau_2 - \tau_1|)}{2(T + \tau_1)} \tag{28b}$$

By combining (28a) and (28b), we obtain

$$(1 - 2k_a - 2Tk_r\tau_1)h - 2(T + \tau_1) - [Tk_r + k_r\tau_1 + 2k_rk_a\Big|\tau_2 - \tau_1\Big|]h^2 > 0 \tag{29}$$

Due to that $Tk_r + k_r\tau_1 + 2k_rk_a|\tau_2 - \tau_1| > 0$, (29) is reduced to

$$(1 - 2k_a - 2Tk_r\tau_1)h - 2(T + \tau_1) > 0 \tag{30}$$

After some simplifications, the bound of the time headway is given by

$$h > h_{\mathrm{A,min}} = \frac{2(T + \tau_1)}{1 - 2k_a - 2Tk_r\tau_1} \tag{31}$$

This completes the proof of Theorem 1. □

Remark 3. *Theorem 1 provides a sufficient condition to guarantee the string stability of the vehicular platoon with sensing delay and communication delay, no matter how large the frequency$\omega$of the leader vehicle's maneuver is. Moreover, Theorem 1 reveals that both the sensing delay and communication delay have a negative impact on the string stability of the platoon and restrict the available ranges of selecting the controller gains k_r, k_v, k_a.*

Remark 4. *Theorem 1 deduces the minimum time headway of the vehicular platoon for $\omega > 0$ when the string stability conditions are satisfied. By taking into account the objective of enhancing road capacity, it is desirable to set the time headway as close as possible to$h_{\mathrm{A,min}}$. By doing so, the platoon can achieve a high level of efficiency in utilizing the available road space while maintaining the string stability.*

In practice, the leader vehicle is unlikely to maneuver with high frequency due to the physical and mechanical constraints. Most of the energy of the spacing errors is in the region of low frequency, so this region is most critical for analyzing the string stability. Next, we only consider the low-frequency maneuver of the leader vehicle, aiming at providing a more practical string stability criterion.

Theorem 2. *For the low frequency ω satisfying $\sin(\tau_k\omega) > 0$ and $\cos(\tau_k\omega) > 0$, $k = 1, 2$, the closed–loop platoon dynamics described by (12) are string–stable if one of the following conditions is satisfied.*

$$\overline{\Delta} < 0 \ \wedge \overline{\beta}_6 > 0 \ \wedge \beta_2 > 0 \tag{32a}$$

$$\overline{\Delta} \geq 0 \ \wedge \overline{\beta}_6 > 0 \ \wedge \overline{\beta}_4 > 0 \ \wedge \beta_2 > 0 \tag{32b}$$

where

$$\begin{cases} \overline{\Delta} = \overline{\beta}_4^2 - 4k_r\overline{\beta}_6\beta_2, \\ \overline{\beta}_6 = T^2 - 2Tk_a\tau_2 - k_a\tau_2^2, \\ \overline{\beta}_4 = 1 - 2Thk_r - 2Tk_v + 2k_a - 2(hk_r + k_v)\tau_1 + \theta, \\ \theta = \begin{cases} 0, & \tau_1 \leq \tau_2 \\ 2hk_rk_a(\tau_1 - \tau_2), & \tau_1 > \tau_2 \end{cases}. \end{cases}$$

With respect to the string stability conditions (32), the bound of the time headway is given by

$$h > h_{\mathrm{L,min}} = \frac{2(T + \tau_1)}{1 + 2k_a} \tag{33}$$

Proof. According to the assumption of Theorem 2, there exist that $\sin(\tau_k\omega) > 0$, $-\sin(\tau_k\omega) > -\tau_k\omega$, $\cos(\tau_k\omega) = 1 - 2\sin^2(0.5\tau_k\omega) > 1 - 0.5\tau_k^2\omega^2$, and $-\cos(\tau_k\omega) > -1$, $k = 1, 2$. Thus, the inequality in (26) can be simplified as

$$|M+N|^2 - |N|^2 \geq \overline{\beta}_6\omega^6 + \overline{\beta}_4\omega^4 + k_r\beta_2\omega^2 \geq 0 \tag{34}$$

When the inequality (34) is established, the string stability conditions for the low frequency ω can be obtained as (32a) and (32b).

Then, for low–frequency maneuver, the bound of the time headway (33) can be deduced from (32b). It is assumed that $\overline{\Delta} \geq 0$ and $\overline{\beta}_6 > 0$. $\overline{\beta}_4 > 0$ and $\beta_2 > 0$ can be rewritten as

$$k_v > \frac{1}{h} - \frac{hk_r}{2} \tag{35a}$$

$$k_v < \frac{1 - 2Thk_r + 2k_a - 2hk_r\tau_1 + \theta}{2(T+\tau_1)} \tag{35b}$$

Since that θ is different for the situations that $\tau_1 < \tau_2$ and $\tau_1 > \tau_2$, these two situations are analyzed as follows, respectively.

Firstly, we consider the situation that $\tau_1 < \tau_2$, i.e., $\theta = 0$. By combining (35a) and (35b), one achieves

$$h(1+2k_a) - 2(T+\tau_1) - h^2k_r(T+\tau_1) > 0 \tag{36}$$

Due to that $T + \tau_1 > 0$, the bound of the time headway for low frequency (33) can be obtained by reorganizing (36).

Secondly, by considering the other situation that $\tau_1 > \tau_2$, i.e., $\theta = 2hk_rk_a(\tau_1 - \tau_2)$, we combine (35a) and (35b) to achieve

$$h(1+2k_a) - 2(T+\tau_1) - h^2k_r[\tau_1 + T - 2k_a(\tau_1 - \tau_2)] > 0 \tag{37}$$

By assuming that $T > (2k_a - 1)\tau_1 - 2k_a\tau_2$, the bound of the time headway can still be represented by (33), which is the same as the result of the situation that $\tau_1 < \tau_2$. Thus, for the above two situations that $\tau_1 < \tau_2$ and $\tau_1 > \tau_2$, the bound of the time headway for low-frequency can be both derived as (33). □

Remark 5. *Theorem 2 provides a sufficient condition to guarantee the string stability of the vehicular platoon for the region of low frequency, in which most of the energy of the spacing errors exists. Compared to Theorem 1 that no matter how large the frequency of the leader vehicle's maneuver is, Theorem 2 is more practical. Theorem 2 relaxes the constraints of the controller gains k_r, k_v, k_a, which can be observed by comparing (32) with (24), so it benefits the controller synthesis for the vehicular platoon with sensing delay and communication delay.*

Remark 6. *By comparing the bound of the time headway for all frequency (25) and that for low frequency (33), it is found that $h_{\mathrm{L,min}}$ in Theorem 2 is smaller than $h_{\mathrm{A,min}}$ in Theorem 1 when $\tau_1 < 2k_a/Tk_r$. It means that the time headway of the vehicular platoon can be further reduced to improve road capacity in practice.*

Remark 7. *The lower bound of the time headway derived in Theorem 2 is similar to the recent research* [29], *but there are distinctions between the two results. In* [29], *on the account of neglecting the impact of low frequency on the string stability, $h_{\mathrm{L,min}}$* is seemed suitable for all frequencies. On the contrary, we reveal that $h_{\mathrm{L,min}}$ just appears at low frequency.

5. Numerical Simulations

In this section, numerical simulations are implemented to verify the correctness of the main results. A vehicular platoon including five followers and one leader is considered under PF topology. The main parameters, including the time constant of the drivetrain [35],

time headway [36], and controller gains [28] are provided in Table 1. These parameters satisfy Lemma 1, so the vehicular platoon is internally stable for the delay–free case.

Table 1. Vehicular platoon and controller parameters.

Parameter	Description	Value	Unit
T	Time constant of the drivetrain	0.4	s
d	Standstill spacing	10	m
h	Time headway	2	s
$v_{\max}$	Maximum velocity	55.6	m/s
$v_{\min}$	Minimum velocity	0	m/s
k_r, k_v, k_a	Controller gains	0.2, 0.9, 0.05	-

In the following, we conduct two types of simulations to evaluate the internal stability and string stability of the vehicular platoon with sensing delay and communication delay.

5.1. Internal Stability Verification

In this simulation, the leader vehicle maneuvers at a constant velocity of 25 m/s (i.e., 90 km/h). By utilizing our proposed internal stability analysis method, the kernel and offspring hypersurfaces of the CTCR diagram are depicted in Figure 3. The kernel hypersurfaces (KHs) and offspring hypersurfaces (OHs) are represented as red and blue, respectively. The stable region is marked as the shaded zone in Figure 3b, which is an exact and exhaustive stability map for the vehicular platoon with sensing delay and communication delay. It is remarked that there is no stable region outside the shaded zone.

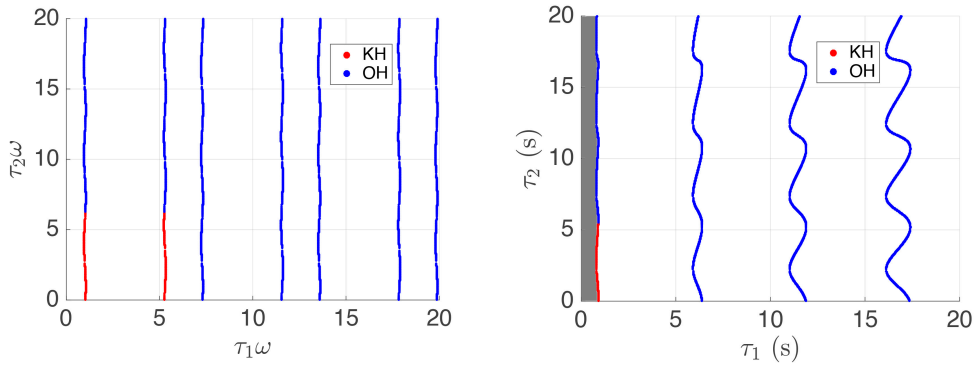
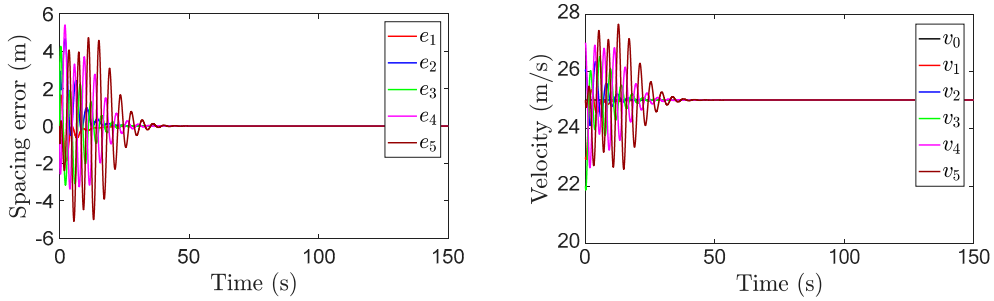


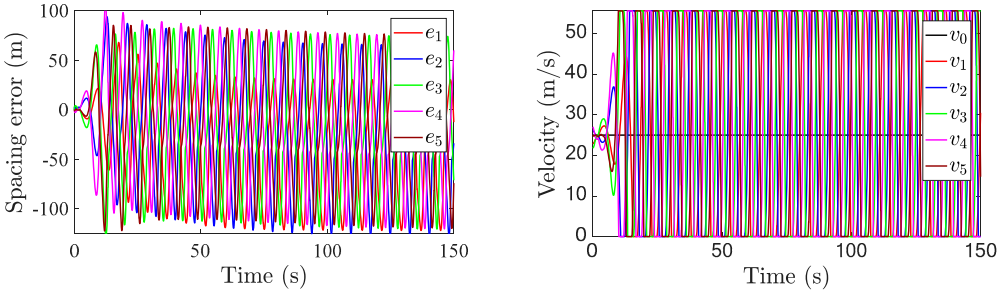
Figure 3. CTCR paradigm of the vehicular platoon: (**a**) Spectral delay space representation. (**b**) Delay space representation.

In order to verify the results, we consider two different points "a" (i.e., $< \tau_1, \tau_2 > = < 0.4$ s, 2 s $>$) and "b" (i.e., $< \tau_1, \tau_2 > = < 2$ s, 2 s $>$), which are inside and outside the stable region, respectively. The spacing error and velocity of the vehicles for the point "a" are exhibited in Figure 4, and those for the point "b" are exhibited in Figure 5. It is seen that the spacing errors and velocities of the follower vehicles converge in Figure 4, such that the internal stability is guaranteed. On the contrary, the spacing errors and velocities diverge in Figure 5, so the instability occurs. Thus, the simulation results verify the effectiveness of our proposed internal stability analysis method.



(**a**) (**b**)

Figure 4. Performance of the vehicular platoon for the point "a": (**a**) Spacing error. (**b**) Velocity.



(**a**) (**b**)

Figure 5. Performance of the vehicular platoon for the point "b": (**a**) Spacing error. (**b**) Velocity.

Furthermore, we compare the computational efficiency of our proposed Dixon resultant matrix–based method to that of the other two state–of–the–art methods, i.e., the Sylvester resultant matrix-based method [21] and ACE combined with Kronecker summation [22]. The three methods are all combined with the CTCR paradigm to compute the ETDMs for the identical vehicular platoon. The three programs are simulated in an identical computer, which has a 2.93 GHz Intel Core 2 Duo and 4 GB RAM, and has Matlab 2017a installed. Simulation time is exhibited in Table 2. It is seen that our proposed method consumes the least simulation time. The simulation time of our proposed method is less than that of the Sylvester resultant matrix–based method by two orders of magnitude, and less than that of ACE combined with Kronecker summation by three orders of magnitude. In conclusion, the computational burden of applying the CTCR paradigm to compute the ETDMs is elegantly reduced by our proposed method.

Table 2. Simulation time.

Method	Simulation Time (min)
The proposed method	0.05
Sylvester resultant matrix–based method in [21]	2.1
ACE combined with Kronecker summation in [22]	27.3

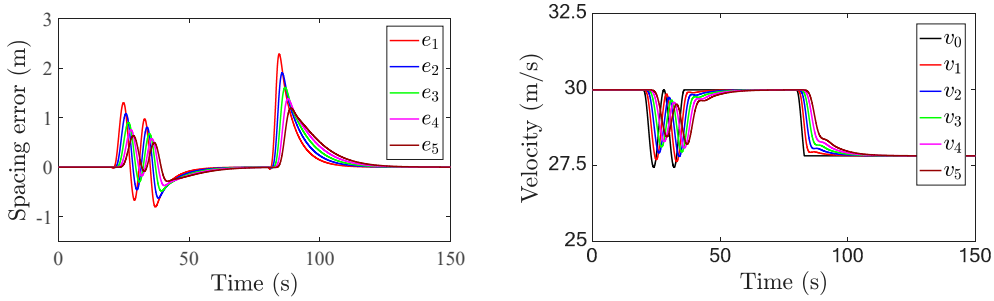
5.2. String Stability Verification

The main results of the string stability conditions and the bound of the time headway derived in Theorem 1 and Theorem 2 are verified in Case 1 and Case 2, respectively. The sensing delay and communication delay are set as $< \tau_1, \tau_2 > = < 0.01 \text{ s}, 0.1 \text{ s} >$, which satisfy the string stability conditions (24b) and (32b) with the parameters in Table 1. Meanwhile, the acceleration and deceleration of the leader vehicle are considered as the perturbations of the vehicular platoon.

Case 1: The sinusoidal perturbations are applied as the acceleration of the leader vehicle, which are arranged as

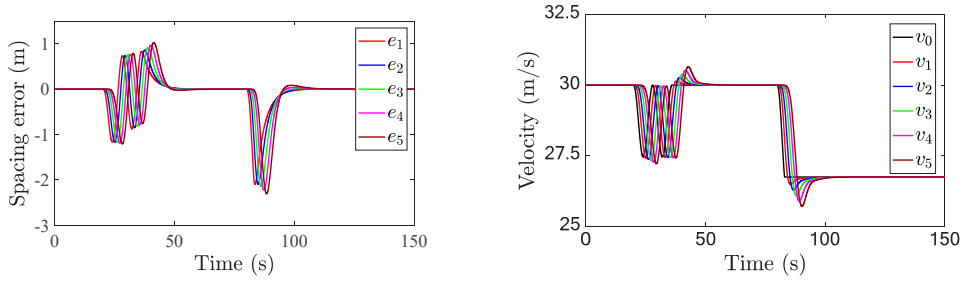
$$a_0(t) = \begin{cases} \sin(\frac{\pi}{4}t)\ \mathrm{m/s^2}, & 20\ \mathrm{s} \le t \le 36\ \mathrm{s} \\ -2\sin(\frac{\pi}{4}t)\ \mathrm{m/s^2}, & 80\ \mathrm{s} \le t \le 96\ \mathrm{s} \\ 0, & \text{otherwise.} \end{cases} \tag{38}$$

With the vehicular platoon and controller parameters in Table 1, the bound of the time headway (25) is $h_{\mathrm{A,min}} = 0.9127$ s. To satisfy the string stability conditions derived in Theorem 1, we set the time headway as $h = 1.5964\ \mathrm{s} > h_{\mathrm{A,min}}$. The performance of the vehicular platoon is given in Figure 6. It is seen that the spacing errors decay when propagating along the vehicle string, which illustrates the correctness of the string stability conditions proposed in Theorem 1. On the other hand, by choosing $h = 0.7764\ \mathrm{s} < h_{\mathrm{A,min}}$, the string stability of the vehicular platoon can not be guaranteed, as shown in Figure 7. Thus, the bound of the time headway (25) is valid.



(**a**) (**b**)

Figure 6. Performance of the vehicular platoon with $h > h_{\mathrm{A,min}}$: (**a**) Spacing error. (**b**) Velocity.



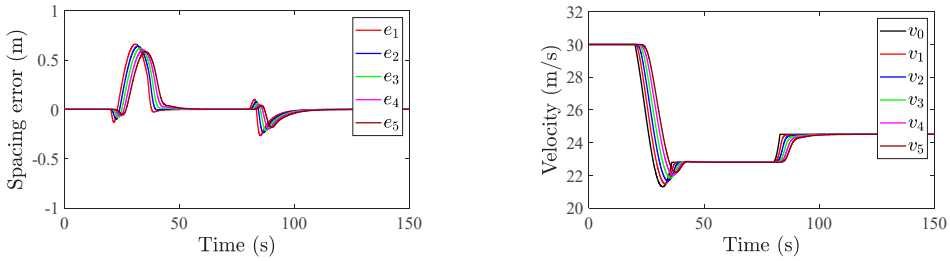
(**a**) (**b**)

Figure 7. Performance of the vehicular platoon with $h < h_{\mathrm{A,min}}$: (**a**) Spacing error. (**b**) Velocity.

Case 2: To examine the main results proposed in Theorem 2, we reduce the frequency of the perturbations from 1/4 rad/s to 1/16 rad/s, and hence the low–frequency perturbations are given by

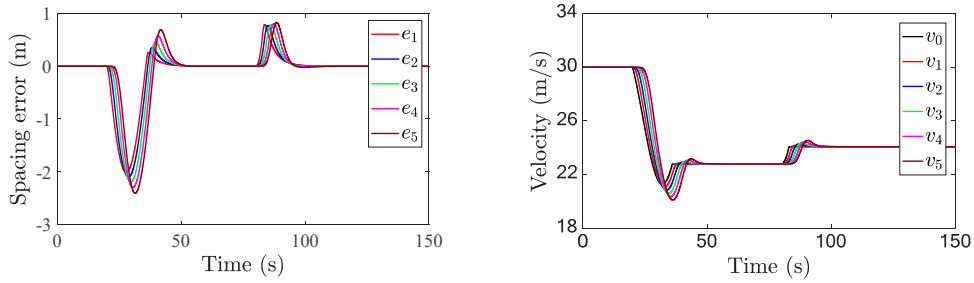
$$a_0(t) = \begin{cases} \sin(\frac{\pi}{16}t)\ \mathrm{m/s^2}, & 20\ \mathrm{s} \le t \le 36\ \mathrm{s} \\ -2\sin(\frac{\pi}{16}t)\ \mathrm{m/s^2}, & 80\ \mathrm{s} \le t \le 96\ \mathrm{s} \\ 0, & \text{otherwise.} \end{cases} \tag{39}$$

Compared to Case 1, the bound of the time headway for low frequency (33) can be reduced to $h_{\mathrm{L,min}} = 0.7455$ s. The time headway is set as $h = 0.7746\ \mathrm{s} > h_{\mathrm{L,min}}$ in Case 2, which is unavailable to guarantee the string stability according to Theorem 2. Then, for the vehicular platoon with the low–frequency perturbations, the spacing errors are attenuated among the followers, as shown in Figure 8. The result illustrates that a lower time headway can be used to hold the string stability for the low–frequency perturbations. After that, by choosing that $h = 0.5432\ \mathrm{s} < h_{\mathrm{L,min}}$, the vehicular platoon is not string–stable in Figure 9. Thus, the string stability conditions and the lower bound of the time headway derived in Theorem 2 are validated as effective.



(**a**) (**b**)

Figure 8. Performance of the vehicular platoon influenced by low–frequency perturbations with $h_{\mathrm{L,min}} < h < h_{\mathrm{A,min}}$: (**a**) Spacing error. (**b**) Velocity.



(**a**) (**b**)

Figure 9. Performance of the vehicular platoon influenced by low–frequency perturbations with $h < h_{\mathrm{L,min}}$: (**a**) Spacing error. (**b**) Velocity.

Case 3: In this case, the leader vehicle undergoes the "acceleration–cruise–brake" scenario, which is more commonly used in the real world. The acceleration and deceleration of the leader vehicle are given by

$$a_0(t) = \begin{cases} 1\ \mathrm{m/s^2}, & 20\ \mathrm{s} \le t \le 23\ \mathrm{s} \\ -2\ \mathrm{m/s^2}, & 80\ \mathrm{s} \le t \le 83\ \mathrm{s} \\ 0, & \text{otherwise.} \end{cases} \tag{40}$$

It is obvious that the acceleration and deceleration of the leader vehicle in this scenario are the low–frequency perturbations. Thus, the time headway is set as $h = 0.7746\ \mathrm{s} > h_{\mathrm{L,min}}$, which is available to guarantee the string stability. To demonstrate the practical significance of our proposed results for the vehicular platoon control, an additional simulation is performed under the above three cases from the perspective of the tracking performance and ride comfort, where the string stability conditions are satisfied. The definitions of the above performances are designed according to [37].

Tracking performance:

$$J_{Ti} = \omega_e \sum_{t=0}^{\infty} e_i^2(t) + \omega_v \sum_{t=0}^{\infty} (v_i(t) - v_{i-1}(t))^2 \tag{41}$$

Ride comfort:

$$J_{Ci} = \omega_c \sum_{t=0}^{\infty} \left(\dot{a}_i(t)\right)^2 \tag{42}$$

where $\omega_e = 0.01$, $\omega_v = 0.01$, and $\omega_c = 0.001$ are the weighting parameters of the spacing error, relative velocity, and derivative of acceleration, respectively.

Table 3 shows the simulation results of the above three cases. For the tracking performance, the values under the three cases decrease with the vehicle index, illustrating that the spacing errors and relative velocity errors decrease upstream, which also states that the vehicular platoon is string-stable. Then, one can see that the values of J_{Ti} and J_{Ci} of Case 2 are smaller than that of Case 1. This means that when subjected to the sinusoidal

perturbations, the vehicular platoon for low frequency has better properties in the tracking performance and ride comfort than that for high frequency. Moreover, the values of J_{Ti} and J_{Ci} of Case 2 are smaller than those of Case 3. This means that when subjected to low frequency, the vehicular platoon under the sinusoidal perturbations exhibits better performance indicators than that in the "acceleration–cruise–brake" scenarios. The above statistical evaluation is conducted on the vehicular platoon that satisfies the string stability conditions in the three different scenarios, and indicates the practical significance of our proposed results for the vehicular platoon control.

Table 3. The tracking performance and ride comfort in the different scenarios.

Vehicle Index	Tracking Performance			Ride Comfort		
	Case 1	Case 2	Case 3	Case 1	Case 2	Case 3
1	46.4875	14.9060	23.2915	0.5238	0.1196	0.5120
2	35.3689	13.6805	22.3953	0.2825	0.0748	0.3605
3	27.9918	12.6983	22.0915	0.1614	0.0557	0.2972
4	22.9289	11.8603	22.0800	0.0949	0.0442	0.2593
5	19.3520	11.1278	22.0581	0.0568	0.0363	0.2345

6. Conclusions

For a vehicular platoon in the presence of sensing delay and communication delay, this paper deduces a necessary and sufficient internal stability condition and two types of sufficient string stability conditions. In the internal stability analysis, the ETDMs are obtained by revealing the kernel and offspring hypersurfaces of the CTCR paradigm, in which the Dixon resultant is utilized instead of the well–known Sylvester resultant, and then the computational burden is reduced significantly. The strength of our proposed method is exhibited by comparative simulation that the simulation time of our proposed method of computing the ETDMs is just 0.05 min, which is less than that of the Sylvester resultant matrix–based method by two orders of magnitude, and less than that of ACE combined with Kronecker summation by three orders of magnitude. In the string stability analysis, we provide the results for the situation no matter how large the frequency of the leader vehicle's maneuver is. Furthermore, a more practical string stability condition is studied by considering only the region of low frequency, where most of the energy of the spacing errors exists. Based on this, a lower bound of the time headway is deduced for low frequency, which can be used to increase road capacity and decrease fuel consumption. Simulation results show that in different scenarios, the spacing errors propagate along the vehicular platoon without divergence when the time headways are larger than our proposed bounds.

In this article, we focus on conducting the stability analysis of the homogeneous vehicular platoon with the sensing delay and communication delay. However, vehicular platoons on the real–world roads may be composed of different types of vehicles. Hence, our future work is to analyze the internal and string stability of the heterogeneous vehicular platoon with the sensing delay and communication delay.

Author Contributions: Conceptualization—writing, X.Z.; Writing—editing, Y.S.; Methodology—validation, Z.Z.; Supervision, M.Y. All authors have read and agreed to the published version of the manuscript.

Funding: This research was funded by the National Natural Science Foundation (NNSF) of China under Grant 62003054, the Key Research and Development Plan of Shaanxi Province under Grant 2023YBGY398, and the Fundamental Research Funds for the Central Universities of China under Grant 300102320109.

Institutional Review Board Statement: Not applicable.

Informed Consent Statement: Not applicable.

Data Availability Statement: Not applicable.

Conflicts of Interest: The authors declare no conflict of interest.

References

1. Ma, K.; Wang, H.; Ruan, T. Analysis of road capacity and pollutant emissions: Impacts of connected and automated vehicle platoons on traffic flow. *Phys. A* **2021**, *583*, 126301–126311.
2. Ploeg, J.; Semsar-Kazerooni, E.; Medina, A.I.M.; de Jongh, J.F.C.M.; van de Sluis, J.; Voronov, A.; Englund, C.; Bril, R.J.; Salunkhe, H.; Arrue, A.; et al. Cooperative automated maneuvering at the 2016 grand cooperative driving challenge. *IEEE Trans. Intell. Transp. Syst.* **2017**, *19*, 1213–1226. [CrossRef]
3. Li, Y.; Zhong, Z.; Song, Y.; Sun, Q.; Sun, H.; Hu, S.; Wang, Y. Longitudinal platoon control of connected vehicles: Analysis and verification. *IEEE Trans. Intell. Transp. Syst.* **2022**, *23*, 4225–4235.
4. Chehardoli, H.; Ghasemi, A. Robust adaptive consensus of decentralized large-scale bi-directional vehicular platoons with only relative position measurement. *IEEE Trans. Veh. Technol.* **2021**, *71*, 1363–1371. [CrossRef]
5. Feng, S.; Zhang, Y.; Li, S.E.; Cao, Z.; Liu, H.X.; Li, L. String stability for vehicular platoon control: Definitions and analysis methods. *Annu. Rev. Control* **2019**, *47*, 81–97.
6. Guo, G.; Li, P.; Hao, L. A new quadratic spacing policy and adaptive fault-tolerant platooning with actuator saturation. *IEEE Trans. Intell. Transp. Syst.* **2020**, *23*, 1200–1212. [CrossRef]
7. Zhang, J.; Ma, X.; Jiang, Q. A geometric approach to analysing the effects of time delays on stability of vehicular platoons with ring interconnections. *Peer Peer Netw. Appl.* **2022**, *15*, 2542–2556. [CrossRef]
8. Jia, D.; Ngoduy, D. Platoon based cooperative driving model with consideration of realistic inter-vehicle communication. *Transp. Res. Part C-Emerg. Technol.* **2016**, *68*, 245–264.
9. Huang, D.; Li, S.; Zhang, Z.; Liu, Y.; Mi, B. Design and analysis of longitudinal controller for the platoon with time-varying delay. *IEEE Trans. Intell. Transp. Syst.* **2022**, *23*, 23628–23639. [CrossRef]
10. Salvi, A.; Santini, S.; Valente, A.S. Design, analysis and performance evaluation of a third order distributed protocol for platooning in the presence of time-varying delays and switching topologies. *Transp. Res. Part C-Emerg. Technol.* **2017**, *80*, 360–383. [CrossRef]
11. Petrillo, A.; Pescape, A.; Santini, S. A secure adaptive control for cooperative driving of autonomous connected vehicles in the presence of heterogeneous communication delays and cyberattacks. *IEEE Trans. Cybern.* **2020**, *51*, 1134–1149. [CrossRef] [PubMed]
12. Shi, M.; Yu, Y.; Xu, Q. Delay-dependent consensus condition for a class of fractional-order linear multi-agent systems with input time-delay. *Int. J. Syst. Sci.* **2019**, *50*, 669–678. [CrossRef]
13. Chen, J.; Liang, H.; Li, J.; Lv, Z. Connected automated vehicle platoon control with input saturation and variable time headway strategy. *IEEE Trans. Intell. Transp. Syst.* **2020**, *22*, 4929–4940. [CrossRef]
14. Chehardoli, H.; Homaeinezhad, M.R.; Ghasemi, A. Control design and stability analysis of homogeneous traffic flow under time delay: A new spacing policy. *Proc. Inst. Mech. Eng. Part D J. Automob. Eng.* **2019**, *233*, 622–635. [CrossRef]
15. Fazelinia, H.; Sipahi, R.; Olgac, N. Stability robustness analysis of multiple time-delayed systems using "building block" concept. *IEEE Trans. Autom. Control* **2007**, *52*, 799–810.
16. Chehardoli, H.; Ghasemi, A.; Najafi, A. Centralized and decentralized distributed control of longitudinal vehicular platoons with non-uniform communication topology. *Asian J. Control* **2019**, *21*, 2691–2699. [CrossRef]
17. Chehardoli, H.; Homaeinezhad, M.R. Third-order leader-following consensus protocol of traffic flow formed by cooperative vehicular platoons by considering time delay: Constant spacing strategy. *Proc. Inst. Mech. Eng. Part I J. Syst Control Eng.* **2018**, *232*, 285–298. [CrossRef]
18. Chehardoli, H.; Ghasemi, A. Formation control of longitudinal vehicular platoons under generic network topology with heterogeneous time delays. *J. Vib. Control* **2019**, *25*, 655–665. [CrossRef]
19. Akkaya, S.; Akbati, O.; Ergenc, A.F. Stability analysis of connected vehicles with V2V communication and time delays: CTCR method via Bézout's resultant. *Trans. Inst. Meas. Control* **2021**, *43*, 1802–1829. [CrossRef]
20. Ghasemi, A.; Rouhi, S. Stability analysis of a predecessor-following platoon of vehicles with two time delays. *Promet* **2015**, *27*, 35–46. [CrossRef]
21. Cepeda-Gomez, R.; Olgac, N. Stability of formation control using a consensus protocol under directed communications with two time delays and delay scheduling. *Int. J. Syst. Sci.* **2016**, *47*, 433–449. [CrossRef]
22. Cepeda-Gomez, R. Finding the exact delay bound for consensus of linear multi-agent systems. *Int. J. Syst. Sci.* **2016**, *47*, 2598–2606. [CrossRef]
23. Liu, Y.; Gao, H.; Zhai, C.; Xie, W. Internal stability and string stability of connected vehicle systems with time delays. *IEEE Trans. Intell. Transp. Syst.* **2020**, *22*, 6162–6174. [CrossRef]
24. Gong, J.; Cao, J.; Zhao, Y.; Wei, Y.; Guo, J.; Huang, W. Sampling-based cooperative adaptive cruise control subject to communication delays and actuator lags. *Math. Comput. Simul.* **2020**, *171*, 13–25. [CrossRef]
25. Hu, S.G.; Wen, H.Y.; Xu, L.; Fu, H. Stability of platoon of adaptive cruise control vehicles with time delay. *Transp. Lett.* **2019**, *11*, 506–515. [CrossRef]

26. Xing, H.; Ploeg, J.; Nijmeijer, H. Padé approximation of delays in cooperative ACC based on string stability requirements. *IEEE Trans. Intell. Veh.* **2016**, *1*, 277–286. [CrossRef]
27. Xiao, L.; Gao, F. Practical string stability of platoon of adaptive cruise control vehicles. *IEEE Trans. Intell. Transp. Syst.* **2011**, *12*, 1184–1194. [CrossRef]
28. Bian, Y.; Zheng, Y.; Ren, W.; Li, S.E.; Wang, J.; Li, K. Reducing time headway for platooning of connected vehicles via V2V communication. *Transp. Res. Part C-Emerg. Technol.* **2019**, *102*, 87–105. [CrossRef]
29. Abolfazli, E.; Besselink, B.; Charalambous, T. On time headway selection in platoons under the MPF topology in the presence of communication delays. *IEEE Trans. Intell. Transp. Syst.* **2021**, *23*, 8881–8894. [CrossRef]
30. Öncü, S.; Ploeg, J.; Van De Wouw, N.; Nijmeijer, H. Cooperative adaptive cruise control: Network-aware analysis of string stability. *IEEE Trans. Intell. Transp. Syst.* **2014**, *15*, 1527–1537. [CrossRef]
31. Paláncz, B.; Zaletnyik, P.; Awange, J.L.; Grafarend, E.W. Dixon resultant's solution of systems of geodetic polynomial equations. *J. Geod.* **2008**, *82*, 505–511. [CrossRef]
32. Ergenc, A.F.; Olgac, N.; Fazelinia, H. Extended Kronecker summation for cluster treatment of LTI systems with multiple delays. *SIAM J. Control Optim.* **2007**, *46*, 143–155. [CrossRef]
33. Sipahi, R.; Olgac, N. Kernel and offspring concepts for the stability robustness of multiple time delayed systems (MTDS). *J. Dyn. Syst. Meas. Control-Trans. ASME* **2007**, *129*, 245–251. [CrossRef]
34. Sönmez, Ş.; Ayasun, S.; Nwankpa, C.O. An exact method for computing delay margin for stability of load frequency control systems with constant communication delays. *IEEE Trans. Power Syst.* **2015**, *31*, 370–377. [CrossRef]
35. Yu, G.; Wong, P.K.; Huang, W.; Zhao, J.; Wang, X.; Yang, Z. Distributed adaptive consensus protocol for connected vehicle platoon with heterogeneous time-varying delays and switching topologies. *IEEE Trans. Intell. Transp. Syst.* **2022**, *23*, 17620–17631. [CrossRef]
36. Alsuhaim, A.; Rayamajhi, A.; Westall, J.; Martin, J. Adapting time headway in cooperative adaptive cruise control to network reliability. *IEEE Trans. Veh. Technol.* **2021**, *70*, 12691–12702. [CrossRef]
37. Li, S.E.; Li, K.; Rajamani, R.; Wang, J. Model predictive multi-objective vehicular adaptive cruise control. *IEEE Trans. Control Syst. Technol.* **2010**, *19*, 556–566. [CrossRef]

Disclaimer/Publisher's Note: The statements, opinions and data contained in all publications are solely those of the individual author(s) and contributor(s) and not of MDPI and/or the editor(s). MDPI and/or the editor(s) disclaim responsibility for any injury to people or property resulting from any ideas, methods, instructions or products referred to in the content.